5-1-2005

A magnetically driven PDMS micropump with ball check-valves

Tingrui Pan
University of Minnesota

Scott J. McDonald
University of Minnesota

Eleanor M. Kai
University of Minnesota

Babak Ziaie
Birck Nanotechnology Center, Purdue University, bziaie@purdue.edu

INSTITUTE OF PHYSICS PUBLISHING JOURNAL OF MICROMECHANICS AND MICROENGINEERING

J. Micromech. Microeng. **15** (2005) 1021–1026 doi:10.1088/0960-1317/15/5/018

A magnetically driven PDMS micropump with ball check-valves

Tingrui Pan[1], **Scott J McDonald**[2], **Eleanor M Kai**[1] **and Babak Ziaie**[1,3]

[1] Department of Electrical and Computer Engineering, University of Minnesota, Minneapolis, MN, USA
[2] Institute of Technology, University of Minnesota, Minneapolis, MN, USA
[3] School of Electrical and Computer Engineering, Purdue University, West Lafayette, IN, USA

Received 28 October 2004, in final form 10 February 2005
Published 30 March 2005
Online at stacks.iop.org/JMM/15/1021

Abstract

In this paper, we present a low-cost, PDMS-membrane micropump with two one-way ball check-valves for lab-on-a-chip and microfluidic applications. The micropump consists of two functional PDMS layers, one holding the ball check-valves and an actuating chamber, and the other covering the chamber and holding a miniature permanent magnet on top for actuation. An additional PDMS layer is used to cover the top magnet, and thereby encapsulate the entire device. A simple approach was used to assemble a high-performance ball check-valve using a micropipette and heat shrink tubing. The micropump can be driven by an external magnetic force provided by another permanent magnet or an integrated coil. In the first driving scheme, a small dc motor (6 mm in diameter and 15 mm in length) with a neodymium–iron–boron permanent magnet embedded in its shaft was used to actuate the membrane-mounted magnet. This driving method yielded a large pumping rate with very low power consumption. A maximum pumping rate of 774 μL min^{-1} for deionized water was achieved at the input power of 13 mW, the highest pumping rate reported in the literature for micropumps at such power consumptions. Alternatively, we actuated the micropump with a 10-turn planar coil fabricated on a PC board. This method resulted in a higher pumping rate of 1 mL min^{-1} for deionized water. Although more integratable and compact, the planar microcoil driving technique has a much higher power consumption.

(Some figures in this article are in colour only in the electronic version)

1. Introduction

Microvalves and micropumps are considered to be key functional components in microfluidic systems. Over the past decade with an increasing interest in the development of biochemical microsystems, there have been numerous reports on the design and fabrication of a variety of microvalves and micropumps. Microvalves can be classified into two types: passive and active, depending on whether they use an external energy source for their operation [1, 2]. Passive valves operate based on the pressure gradient and are often used as check-valves for micropumps, while active valves require outside actuation (e.g., electrostatic, electromagnetic, thermal expansion, thermopneumatic, pneumatic, piezoelectric and shape memory alloy). Micropumps have generally been developed in three different categories, i.e., electroosmotic, positive-displacement and peristaltic [1–13]. Depending on working fluid type, required pumping rate and desired backpressure, various actuation mechanisms and fabrication techniques have been employed. Electroosmotic pumps have the advantage of high backpressures and simple design, but they require very high voltages and a charged working liquid (alternatively, one can pump an uncharged liquid if a charged contact surface can be provided). Peristaltic pumps have also been demonstrated using different fabrication and actuation techniques such as thermopneumatic, piezoelectric,

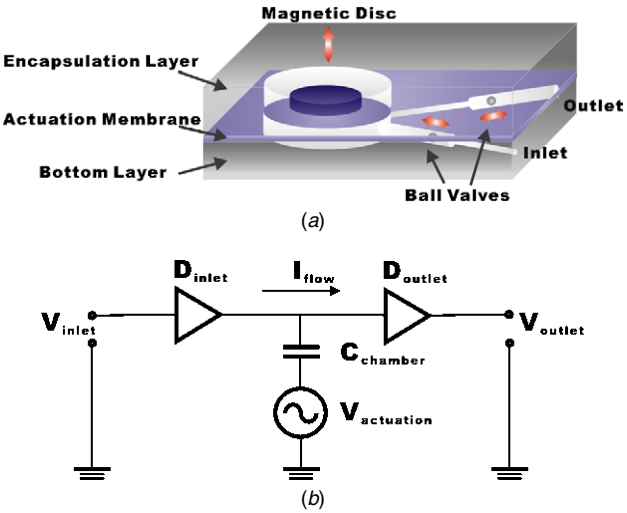

Figure 1. (*a*) A perspective view of the ball-valve PDMS micropump along with (*b*) its equivalent circuit diagram [15].

electrostatic and magnetic. However, they usually have relatively small pumping rates, low backpressures and require a rather complex driving circuitry. Positive-displacement pumps, with the exception of nozzle-diffuser designs, require complex fabrication methods for creating two check-valves and an actuation chamber. Overall, three main drawbacks associated with current micropumps include: (1) fabrication complexity, (2) cost and (3) power consumption. A recent paper on micropumps by Laser and Santiago provides a more detailed review on various pumping schemes and structures [14].

In this paper, we report on the design, fabrication and test of a magnetically actuated positive-displacement PDMS micropump addressing all of the above concerns. Figure 1 shows a perspective view of the PDMS micropump along with its equivalent circuit diagram [15]. In this diagram, the two diodes simulate the one-way performance of the passive check-valves. The ac voltage represents the periodic up-and-down performance of the actuating membrane. The frequency of the membrane movement (f) and effective chamber volume change (V) directly determine the pumping rate (Q), which follows a simple linear relationship: $Q = fV$, though the effective chamber volume change is pressure-dependent. The micropump consists of only two functional PDMS layers; a bottom layer incorporating two ball check-valves and an actuation chamber, and a top flat layer covering the chamber and holding a neodymium–iron–boron (NeFeB) permanent magnetic disc (Magnetic Sensor Systems, CA) used for actuation. An additional PDMS layer is used to cover the top magnet, and thereby encapsulate the entire system. Two magnetic driving schemes can be used to actuate this pump. The micropump can be driven by an external magnetic force provided by (1) another permanent magnet, or (2) an integrated planar microcoil. In the first scheme, a miniature dc motor with an external magnet embedded in its shaft can be used to pull down the NeFeB magnet and actuate the micropump. As discussed in section 4, this method provides a relatively large pumping rate with very low power consumption (basically determined by the load on the dc micromotor). By controlling the motor driving voltage, one can vary the rotation speed and therefore control and adjust the pump performance (pumping rate and backpressure). Using an integrated planar microcoil as the micropump drive has the advantage of being more compact. However, this is at the expense of much higher power consumptions. For the purpose of clarity, in the following sections, we call the two aforementioned driving schemes '*micromotor-drive*' and '*microcoil-drive*'.

As will be shown in the following sections, the pumping rates achieved in our designs range from 100 μL min^{-1} to 1 mL min^{-1}. Micropumps operating at these rates are particularly useful in applications such as (1) handheld devices for environmental sampling, e.g., water pollution measurement and bacterial detection, (2) infusion pumps for bed-side and ambulatory drug delivery and (3) disposable lab-on-a-chip systems for chemical and biological analysis. Many of these applications can benefit from a low cost, low power consumption and high flow rate micropump.

2. Design and fabrication

2.1. Assembly of one-way ball check-valves

The one-way behavior of check-valves significantly affects pumping performance of a positive-displacement pump, e.g., valve leakage reduces backpressure and pumping rate. A novel micropipette–microtube molding technique is used to fabricate the ball check-valves. Figure 2 illustrates the basic components, assembling process, and final packaging of the valves. First, a tapered tube having an inner diameter (ID) of 0.7 mm at the narrow end and 1.2 mm at the wide end is cut from a plastic micropipette. Then, a small stainless steel microsphere (diameter = 0.8 mm, grade = 24, and sphericity = 0.6 μm, Small Parts Inc., FL) is introduced into the tube. A short piece of a Teflon^{TM} tubing (ID = 0.56 mm, OD = 1.1 mm) is cut at a 45° angle at one end and is then inserted into the wide end of the tapered tube. This piece acts as a stopper for the microsphere motion. Finally, two simple microtubes are connected to each side of the tapered micropipette and sealed by polyolefin heat shrink jackets at 150 °C. Using this technique, one can easily achieve a one-way ball valve in a tapered tubing structure with microfluidic tube connections, utilizing its low cost and easily reproducible design.

2.2. Molding of micropump

Figure 3 shows an expanded diagram of the PDMS micropump with two driving schemes. Silicone elastomer (Silgard 184, Dow Corning Corp., MI) was the main structural material used for the body of the pump. The bottom layer was molded to incorporate one actuating chamber and two assembled ball check-valves with microfluidic connectors. The top layer was simply a thin sheet used as the actuation membrane and did not require any mold. Two ball check-valves were fabricated as mentioned in the previous section and horizontally placed into a mold which also held a 1.0 mm thick metallic disc (i.e., the mold of actuation chamber). This configuration results in a lower flow resistance and smaller overall dimensions, as compared with the other alternative, i.e., vertical placement. The valves were orientated so that they would both allow liquid to flow in one direction and block the back flow in the opposite direction. In addition, smooth surfaces of steel ball

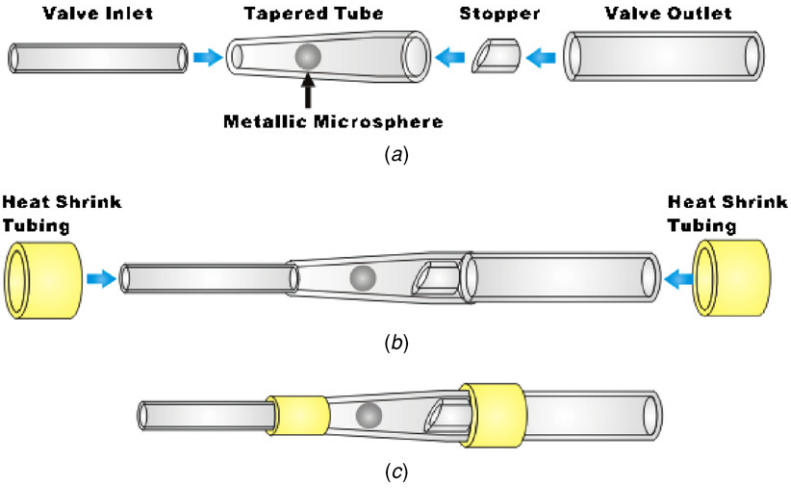

Figure 2. Illustration of (*a*) basic components, (*b*) assembling process and (*c*) final packaging of the micro-ball valve (not to scale).

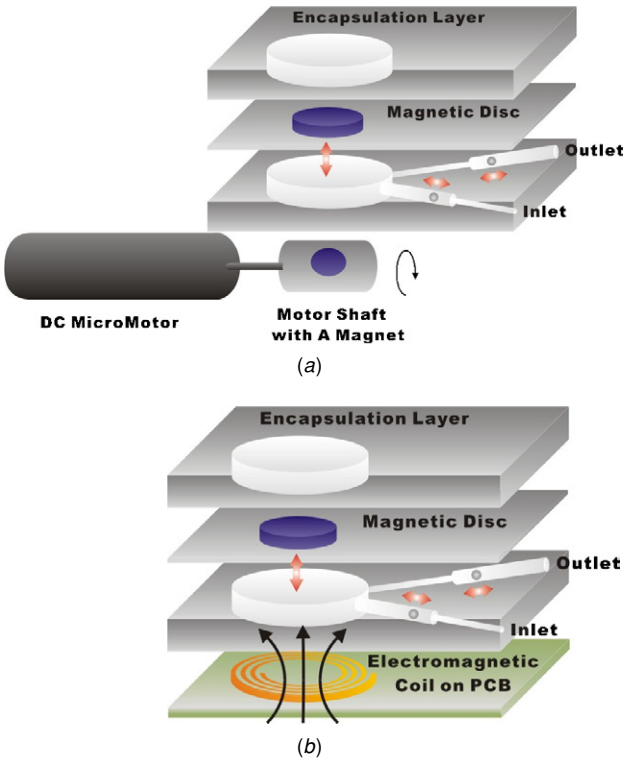

Figure 3. Expanded diagram of the PDMS micropump with two driving schemes: (*a*) *micromotor-drive* and (*b*) *microcoil-drive*.

and tapered tube provide little resistance to the movement of the ball. Subsequently, PDMS (Silgard 184, 10:1 ratio) was poured over the mold of 1.5 mm thick and cured at 100 °C in an oven for 15 min. After curing, the metallic chamber mold could be easily removed (PDMS is not adhesive to metallic surface), leaving the micro-ball valves in place and creating the actuation chamber. A 100 μm thick layer of PDMS was prepared and cured onto a flat surface to serve as the actuation membrane. To bond the actuation membrane to the bottom layer, two different methods were employed. In the first approach, a very thin film of uncured PDMS was applied to the bonding surface of the molded PDMS substrate which was then flipped over and bonded to the thin actuating membrane at a 100 °C oven for 3 min. Alternatively, oxygen plasma treatment (100 W, 13.3 Pa for 30 s) followed by a short curing step (a relative pressure of 100 kPa at 200 °C) was used as a bonding strategy [5]. Both of these methods yield a very strong bond between the two PDMS layers preventing any possible leakage. A NdFeB magnetic disc having a diameter of 3.1 mm and 1.6 mm thick (residual induction $B_r = 12\,900$ Gauss) was finally attached to the actuating membrane right above the center of the actuation chamber using a thin layer of adhesive (0.9 g in weight of the magnetic disc has negligible effect on the membrane deflection compared with external driving forces). The top encapsulating layer and planar coil used in the *microcoil-drive* scheme (10-turn planar copper coil of 200 μm line width machined on a PC board of 35 μm thick copper film) were also bonded using the first technique. The magnetic field strength (B) at 2 mm above the center of the integrated coil, which is the rest position of the actuation magnet, can be also estimated using Biot–Savart's law $B_z = \frac{\mu_0}{4\pi}\frac{2\pi R^2 I}{(z^2+R^2)^{3/2}}$. In addition, a dead volume of 42 μl was measured from the difference in the weight between the 'dry' (without water) and 'wet' (filling with water) states. Finally, an ideal stroke volume (V, i.e., chamber size) of 36 μl was calculated from the dimensions of the mold disc. Figure 4 shows a photograph of the micropump.

3. Experimental setup

In the *micromotor-drive* scheme a miniature dc coreless motor of 6 mm diameter and 15 mm length (MicroMo Electronics Inc., FL) was used to actuate the micropump. For this purpose, a polyvinylsiloxane shaft with an embedded NdFeB permanent magnet (3.1 mm in diameter and 1.6 mm thick, $B =$ 500 Gauss at 2 mm above its surface) was constructed for the micromotor. The pump was then placed on a glass slide that separated it from the micromotor resulting in a 2 mm distance between the external and internal magnets. In the *microcoil-drive* scheme, the pump was powered by a Crown PB-2 power amplifier triggered by a HP 33120A function generator. Using Biot–Savart's law, a magnetic flux density of 10 Gauss is calculated at 2 mm above the center of the integrated coil,

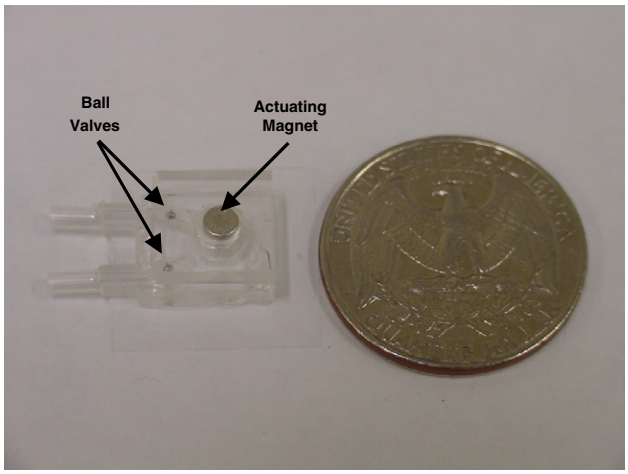

Figure 4. A photograph of the micropump (a US quarter coin is placed for size comparison).

assuming a current of 1.5 A. Although the *micromotor-drive* scheme resulted in a much higher magnetic flux density (B = 500 Gauss) than its *microcoil-drive* counterpart (B = 10 Gauss), since the magnetic field orientation constantly rotates as the motor shaft spins, the actuation time is somehow limited (see the measurement result section). Figure 5 shows the test and measurement setup for both driving configurations.

Deionized (DI) water (density = 1.0 g ml^{-1} and viscosity = 1.025×10^{-3} Pa s at room temperature) and olive oil (density = 0.92 g ml^{-1} and viscosity = 81×10^{-3} Pa s at room temperature) were chosen as the pumping liquids to represent a wide viscosity range. The priming process involved submerging the inlet tube in liquid, and using a mild suction on the outlet to draw-in the fluid and eliminate any air bubble. This priming process is critical to avoid air bubble trapped inside, since any air bubbles in the fluidic channels or actuation chamber will induce surface tension effects and significantly compromise micropump and valve performance.

4. Measurement results

Figure 6 shows leakage measurement results for the ball check-valves. As can be seen, the valves perfectly seal at pressures lower than 5 kPa. A leakage of less than 1 μL min^{-1} is measured between 5 and 30 kPa. Above this threshold pressure of 30 kPa, the valves show a nonlinear behavior with a leakage rate increasing faster than pressure. This can be attributed to the non-ideal circular cross-section of the micropipette and its deformation at high pressures, and the surface roughness and spherical deviation of the steel balls.

Equation (1) is used to obtain the actual rotation speed and frequency of the *micromotor-drive*:

$$V_0 = (I \times R) + V_e = (I \times R) + (\omega \times k_e), \qquad (1)$$

where V_0 and I are the supply voltage and current, V_e is the back EMF, k_e is a EMF constant and R is the terminal resistance. The values for k_e (0.212 mV rpm^{-1}) and R (37.7 Ω) can be obtained from the manufacturer.

To perform the pumping rate test, two additional silicone tubes (ID = 1.5 mm and OD = 1.9 mm) were used to connect the inlet valve to a reservoir and the outlet valve to a measuring

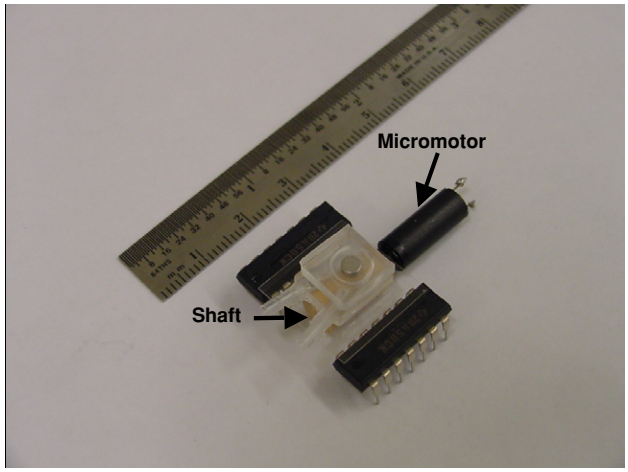

(*a*)

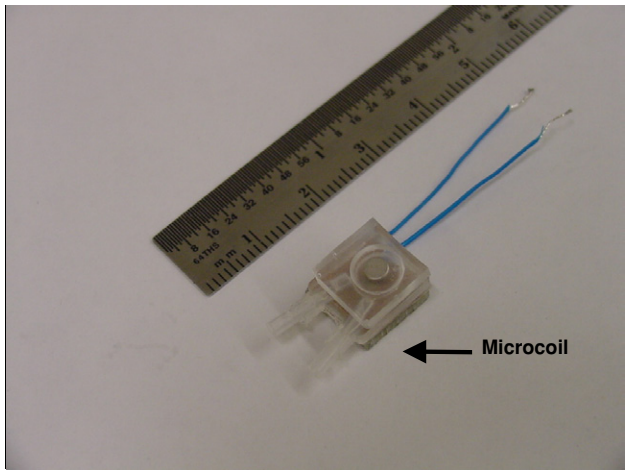

(*b*)

Figure 5. The test and measurement setups of (*a*) *micromotor-drive* and (*b*) *microcoil-drive*.

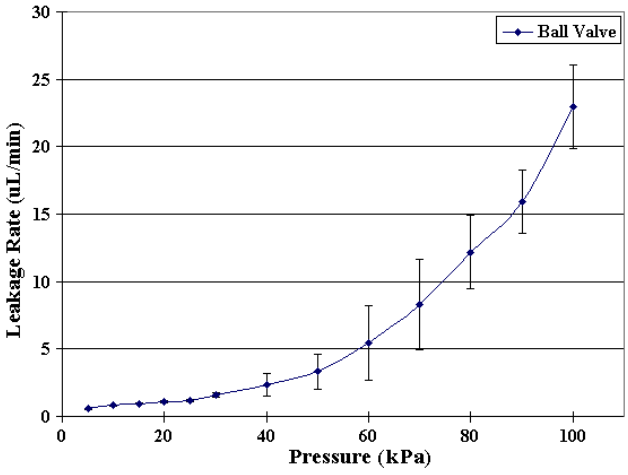

Figure 6. Leakage measurement results of the one-way ball check-valves.

cylinder. Laminar flow in microfluidic devices allows the inlet and outlet fluidic resistances to be directly calculated using Poiseuille's equation: $R = \frac{8\eta L}{\pi r^4}$ (R is the flow resistance, η is the fluid viscosity and L, r are length and radius of

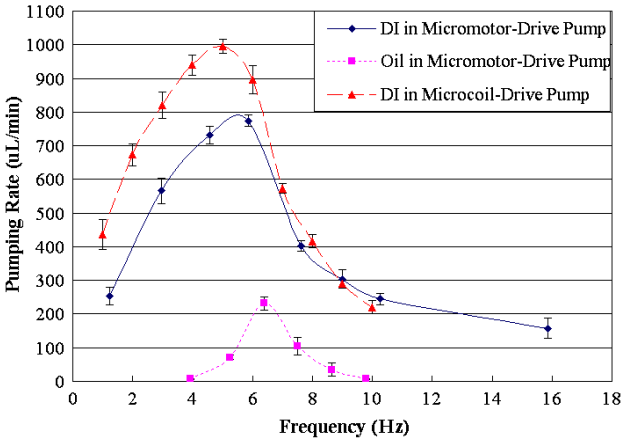

Figure 7. Pumping rate versus motion frequency of the actuating membrane for both driving schemes.

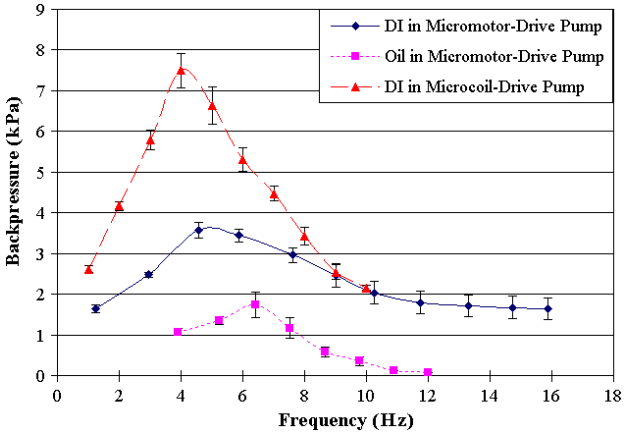

Figure 8. Backpressure versus motion frequency of the actuating membrane for both driving schemes (at zero flow rates).

the cylindrical tube). At the pumping rates concerned here (100 μL min^{-1} to 1 mL min^{-1}), the inlet and outlet flow resistances were negligible (pressure drop of 7.5 Pa at the maximum pumping rate of 1 mL min^{-1} in a 5 mm long inlet or outlet tube) and had no significant influence on the pumping rate and backpressure measurements.

The *micromotor-driven* pump was tested with both DI-water and olive oil whereas the *microcoil-drive* pump was only tested with DI-water. The *microcoil-driven* pump performed poorly with the oil as the working fluid. This is due to the cavitation effects resulting from the heated coil in contact with the oil which has a lower heat capacity and larger viscosity than water (i.e., it is easier to create microbubbles in oil). Figure 7 shows the pumping rate versus the motion frequency of the actuating membrane for both driving schemes. As expected, initially the pumping rate increases parabolically with frequency; then at higher speeds, it reaches a maximum followed by sharp decrease. This parabolic increase in the pumping rates could be explained by the fact that the stroke volume decreases with increasing frequency due to the incomplete closure of actuation chamber. The saturation and the final drop in the pumping rate are mainly due to the mechanical resonance of the actuation membrane structure and inefficiency of the check-valves. Our observations have shown that in a static situation (i.e., placing a magnet underneath the membrane), the top magnet touches the bottom of the channel. In a dynamic case where the bottom magnet is constantly rotating, the deflection depends on the actuation frequency. In addition, since the olive oil is 80 times more viscous than DI-water, it presents a much higher flow resistance resulting in a significant reduction in the pumping rate. We achieved peak flow rates of 774 μL min^{-1} at 5.9 Hz (350 rpm) and 232 μL min^{-1} at 6.4 Hz (384 rpm) for DI-water and olive oil using the *micromotor-drive*. Due to a tighter closure of the actuation chamber when driven by a square waveform, the microcoil-drive can achieve higher peak flow rates (1 mL min^{-1} at 5.0 Hz); however, this is at the expense of higher power consumption (500 mW, compared to 13 mW measured for the *micromotor-drive*). In pumping DI-water, the high power consumption can result in evaporation and bubble generation inside the actuation chamber, thus significantly degrading the performance. Our experiments with integrated microcoil were primarily designed to illustrate the pumping capability and improved performance is achievable using an electromagnetic drive. Power consumption and heating effects can be easily reduced through the fabrication of a multi-layer low-profile solenoid (to increase the magnetic field), although it will be extremely challenging to compete with the *micromotor-driven* pump in power dissipation and efficiency.

We also conducted several tests to measure the pumping backpressure. For these measurements, the inlet needle was connected to a reservoir of water via a primed tube while the outlet needle was connected to a vertical tube used to measure the pumped liquid height. A graph of pumping backpressure (at zero flow rates) versus motion frequency of the actuating membrane for both driving schemes is shown in figure 8. A maximum backpressure of 7.5 kPa (at 4.0 Hz) for DI-water in the *microcoil-driven* pump was measured, while 3.6 kPa (at 4.8 Hz or 286 rpm) and 1.7 kPa (at 6.2 Hz or 373 rpm) were the peak backpressures measured for DI-water and olive oil in the *micromotor-driven* pump, respectively. As can be seen, the actual backpressure is lower than the valve leakage threshold pressure (30 kPa). This is due to the back flow associated with the lag in the closure of the ball check-valve.

It is instructive to compare the performance of the micropump described in this paper with several similar devices in the market and some previously reported micropumps in the literature. Table 1 shows the comparison of key characteristics of several micropumps. Bartels mP5 and ThinXXS MDP1304 are positive-displacement micropumps manufactured by two German companies [16, 17]. The former one is made of plastic layers, while the latter one consists of metal and plastic materials. EsoxPump^{TM} V01 is using a deformed elastomeric membrane to drive the micropump [18]. In addition, Tai's and Quake's groups at CalTech have fabricated a variety of micropumps from silicon and polymer (Parylene and PDMS) [4, 19]. Compared with these pumps, one can point to several advantages associated with our micropumps. These include (1) they are fabricated from inexpensive building materials such as PDMS, micropipette tubing, and stainless steel microspheres, (2) the *microcoil-driven* pump total dimensions are 12 $\times$ 10 $\times$ 5 mm^3 which is one of the smallest among those reported and marketed

Table 1. Key characteristics of several micropumps.

	Pump type	Materials	Dimension	Pumping rate	Backpressure	Power consumption
Bartels mP5 [15]	Positive displacement	Plastic polyphenyl sulphon	$18 \times 15 \times 3$ mm^3	50–3000 μl min^{-1}	50 kPa	45 mW
ThinXXS MDP1304 [16]	Positive displacement	Metal and plastic	$26 \times 25 \times 13$ mm^3	6.0 ml min^{-1}	35 kPa	NA
EsoxPump^{TM} V01 [17]	Pressurized	Steel and polymer	$25 \times 25 \times 7$ mm^3	35–1400 nl min^{-1}	NA	NA
Quake *et al* [18]	Peristaltic	Silicone rubber	NA	141 nl min^{-1}	70 kPa	NA
Tai *et al* [4]	Positive displacement	Polymers and silicon	$\sim 18 \times 18 \times 3$ mm^3	4.5 μl min^{-1}	2.1 kPa	NA
Micromotor-driven pump	Positive displacement	PDMS and motor	$25 \times 10 \times 10$ mm^3	200–800 μl min^{-1}	7.5 kPa	13 mW
Microcoil-driven pump	Positive displacement	PDMS and PCB	$12 \times 10 \times 5$ mm^3	200–1000 μl min^{-1}	3.6 kPa	500 mW

(it still provides a comparable maximum performance such as pumping rate and backpressure) and (3) the *micromotor-driven* pump has one of the lowest power consumption among the micropumps with hundreds of μL min^{-1} pumping rates, although some other pumps, e.g., Bartels mP5, are targeting higher backpressures (50 kPa) and pumping rates (3000 μl min^{-1}).

5. Conclusions

In this paper, we reported on a PDMS membrane micropump with two one-way ball check-valves. The fabrication process includes one simple PDMS molding step with an additional layer of actuating membrane mounted with small permanent magnets. Two driving schemes, *micromotor-drive* and *microcoil-drive*, were investigated. Large pumping rates were achieved in both schemes (hundreds of μL min^{-1}) with the *micromotor-drive* having the lowest power consumption reported in literature. The *microcoil-driven* pump was fully integrated with an even higher pumping rate (1 mL min^{-1}) and back pressures (7.5 kPa, a human heart can generate 13 kPa) at the expense of having much higher power consumption.

Acknowledgments

We would like to thank Dr William Robbins and Emile Davies-Venn for their help in the planar coil fabrication and electromagnetic driving setup. This work is supported by NSF CAREER award BES-0093604 to Dr Babak Ziaie.

References

[1] Beebe D J, Mensing G A and Walker G M 2002 Physics and applications of microfluidics in biology *Annu. Rev. Biomed. Eng.* **4** 261–86

[2] Kovacs G T A 1998 *Micromachined Transducers Sourcebook* (New York: McGraw-Hill)

[3] Accoto D, Carrozza M C and Darlo P 2000 Modelling of micropumps using unimorph piezoelectric actuator and ball valves *J. Micromech. Microeng.* **10** 277–81

[4] Grosjean C and Tai Y C 1999 A thermopneumatic peristaltic micropump *IEEE Transducers Conf. (Sentai, Korea)*

[5] Jo B H, van Lerberghe L M, Motsegood K M and Beebe D J 2000 Three-dimensional micro-channel fabrication in polydimethylsiloxane (PDMS) elastomer *J. Microelectromech. Syst.* **9** 76–81

[6] Khoo M and Liu C 2001 Micro magnetic silicone elastomer membrane actuator *Sensors Actuators* A **89** 259–66

[7] Laser D J, Myers A M, Yao S, Bell K F, Goodson K E, Santiago J G and Kenny T W 2003 Silicon electroosmotic micropumps for integrated circuit thermal management *IEEE Transducers Conf. (Boston, MA)*

[8] Olsson A, Enoksson P, Stemme G and Stemme E 1997 Micromachined flat-walled valveless diffuser pumps *J. Microelectromech. Syst.* **6** 161–6

[9] van de Pol F C M, van Lintel H T G, Elwenspoek M and Fluitman J H J 1990 A thermopneumatic micropump based on microengineering techniques *Sensors Actuators* A **21–3** 198–02

[10] Tsai J and Lin L 2002 A thermal-bubble-actuated micronozzle-diffuser pump *J. Microelectromech. Syst.* **11** 665–71

[11] Yamahata C and Gijs M A M 2004 Plastic micropumps using ferrofluid and magnetic membrane actuation *17th IEEE MEMS Conf. (Maastricht, Netherlands)*

[12] Yamahata C, Lacharme F, Matter J, Schnydrig S, Burri Y and Gijs M A M 2004 Electromagnetically actuated ball valve micropumps, online at http://lmis2.epfl.ch/projects/pdf/41.pdf (accessed on 30 Nov. 2004)

[13] Hatch A, Kamholz A E, Holman G, Yager P and Böhringer K F 2001 A ferrofluidic magnetic micropump *J. Microelectromech. Syst.* **10** 215–21

[14] Laser D J and Santiago J G 2004 A review of micropumps *J. Micromech. Microeng.* **14** R35–R64

[15] Woias P 2001 Micropumps—summarizing the first two decades *Proc. SPIE* **4560** 39–52

[16] Bartels Mikrotechnik, Dortmund, Germany, website: http://www.bartels-mikrotechnik.de

[17] ThinXXS Microtechnology Co, Mainz, Germany, website: http://www.thinxxs.com

[18] Esox Technology Corp, CA, website: http://www.users.uswest.net/∼bwigness/tst_kit.htm.

[19] Unger M A, Chou H P, Thorsen T, Scherer A and Quake S R 2000 Monolithic microfabricated valves and pumps by multilayer soft lithography *Science* **288** 113–6